



HAL
open science

Unexpected frictional behavior of laser-textured hydrophobic surfaces

Hiba Jendoubi, Olga Smerdova, Noël Brunetière

► **To cite this version:**

Hiba Jendoubi, Olga Smerdova, Noël Brunetière. Unexpected frictional behavior of laser-textured hydrophobic surfaces. *Lubricants*, 2021, 9 (3), pp.31. 10.3390/lubricants9030031 . hal-03376141

HAL Id: hal-03376141

<https://hal.science/hal-03376141>

Submitted on 13 Oct 2021

HAL is a multi-disciplinary open access archive for the deposit and dissemination of scientific research documents, whether they are published or not. The documents may come from teaching and research institutions in France or abroad, or from public or private research centers.

L'archive ouverte pluridisciplinaire **HAL**, est destinée au dépôt et à la diffusion de documents scientifiques de niveau recherche, publiés ou non, émanant des établissements d'enseignement et de recherche français ou étrangers, des laboratoires publics ou privés.

Unexpected frictional behavior of laser-textured hydrophobic surfaces

Hiba Jendoubi ¹, Olga Smerdova ¹  and Noël Brunetière ^{1,*} 

¹ Institut Pprime; CNRS, Université de Poitiers, ISAE-ENSMA, Poitiers, France

* Correspondence: noel.brunetiere@univ-poitiers; Tel.: +33-549-496-531

Abstract: Hydrophobic surfaces can allow a liquid to slip over the surface and can thus reduce friction in lubricated contact working in a full film regime. Theory supports that the amount of slip can be increased if super-hydrophobic surfaces that are composed of a textured low surface energy material are used. In this work, polytetrafluoroethylene (PTFE) polymer samples were textured with a femto second laser to create super-hydrophobic surfaces by machining a hexagonal network of small circular holes with 10 and 20 μm lattice sides. The frictional behavior of these surfaces was compared to the smooth PTFE samples. Surprisingly, the textured surfaces revealed higher friction coefficients than the smooth surfaces. This higher friction can be explained by a change of wetting regime due to high pressure in fluid and a possible generation of vortices in the cavities.

Keywords: Surface texture; Hydrophobic surface; Friction; Lubrication

1. Introduction

According to Holmberg and Erdemir [1], about 23% of total global energy consumption is used to fight friction and wear. It is thus essential to propose solutions to reduce friction in machine components. In the case of lubricated contacts, surface texturing has proven to be efficient in several configurations to reduce friction [2,3]. For instance, by creating a network of shallow grooves on the sliding surface, the friction and temperature in a mechanical seal can be reduced by 50 % [4,5].

Another solution to reduce friction was proposed by Spikes [6,7], which uses surfaces on which the lubricant fluid can slip, meaning that there is no adherence between the fluid and the surface. This slip is characterized by the slip length, which is defined as the distance between the surface and the point at which the relative fluid velocity would vanish. Salant and Fortier [8] showed theoretically that performance can be further improved by combining slip and no-slip areas on the surface. The slip area lets more fluid enter the contact, as if the film was thicker. The heterogeneous slip/no slip bearing can thus be compared to a pocket or a step bearing. Several authors have since performed simulations to demonstrate the interest for this type of slip surface [9,10]. It is thus of importance to produce surfaces with slip that can be used in lubricated applications.

In their experimental work, Zhu and Granick [11] demonstrated that fluid can slip on a poorly wetted surface when its roughness height is lower than 6 nm. For lower roughness level, the level of slip, which is characterized by the slip length, is controlled by chemical interactions between the fluid and the surface; as early shown by Schnell [12]. In the case of confined flows, roughness can allow slip of the fluid [13]. Using molecular dynamics, Huang et al. [14] found that the slip length is strongly correlated to the contact angle formed between the solid surface and a sessile water drop. The contact angle characterizes by a simple measurement the intensity of chemical interactions of water with the surface. The slip length is higher when the contact angle is higher. In both studies [11,14], the value of the slip length is a few tens of nanometers. According to theoretical work [6–10], these surfaces could provide lower friction level when used

Citation: Jendoubi, H.; Smerdova, O.; Brunetière, N. Unexpected frictional behavior of laser-textured hydrophobic surfaces. *Lubricants* **2021**, *1*, 0. <https://dx.doi.org/10.3390/lubricants1010000>

Received:

Accepted:

Published:

Publisher's Note: MDPI stays neutral with regard to jurisdictional claims in published maps and institutional affiliations.

Copyright: © 2021 by the authors. Submitted to *Lubricants* for possible open access publication under the terms and conditions of the Creative Commons Attribution (CC BY) license (<https://creativecommons.org/licenses/by/4.0/>).

40 in lubricated contacts. These theoretical findings were confirmed for lubricated contacts
41 submitted to low loads for which Choo et al. [15] found that a lower friction is obtained
42 with hydrophobic surfaces (contact angle higher than 90°) than with hydrophilic surfaces
43 (contact angle lower than 90°). Similarly, Guo et al. [16,17] used several types of coating
44 materials with different contact angles and showed that higher contact angle values lead
45 to a behavior corresponding to slip of the lubricant on the coated surface. **In the case
46 of limit lubrication regime, the combination of a hydrophic and a hydrobobic surfaces
47 in a water lubricated contact is also efficient to reduce friction thanks to an hydration
48 mechanism [18,19]. These very low film thicknesses lubrication corresponding to high
49 loading are however not considered in the present work.**

50 A much higher contact angle can be found on natural materials that are qualified as
51 super-hydrophobic, such as the lotus leaf [20]. A texture is combined with a low surface
52 energy material to give a Cassie Baxter state where the water drop lies on the top of
53 the texture asperities [21]. Ou et al. [22] were able to significantly reduce water flow
54 friction in micro-channels by using textured surface with a surface treatment to reduce
55 surface energy. The slip length of these surfaces was about $20\ \mu\text{m}$. In 2006, Choi and Kim
56 [23] created an artificial superhydrophobic surface composed of sharp silicon asperities
57 covered with a layer of PTFE (PolyTetraFluoroEthylene). They tested the surfaces on
58 a cone-and-plate rheometer and found slip length up to $20\ \mu\text{m}$ with water. If 30 % of
59 glycerin is added to water, the slip length could reach about $50\ \mu\text{m}$. This huge slip length
60 value can be explained by the air trapped between the asperities, which reduces the
61 apparent friction of the fluid on the surface. Different surface texture patterns were
62 tested by Srinivasan et al. [24] on a plate-on-plate rheometer. A slip length of about 40
63 μm was reached in the best case. A summary of the recent research on this topic and the
64 slip length values obtained can be found in the paper of Solomon et al. [25].

65 Super-hydrophobic surfaces appear to be a very attractive solution to reduce friction
66 in lubricated contacts thanks to slip length values that can be higher than the thickness
67 of the lubricating film. However, in the literature, these surfaces were tested in micro-
68 channel flows or in a rheometer where the operating conditions are barely less severe
69 than in lubricated contacts because there is no hydrodynamic pressure generation. In the
70 present work, we designed super-hydrophobic surfaces by texturing flat PTFE samples
71 with a femto second laser [26]. The surfaces were tested on a tribometer with different
72 speeds and load conditions. We then compared the results to untextured surfaces to
73 study the possible friction reduction provided by superhydrophobic textured surface in
74 hydrodynamic lubrication regime.

75 **2. Materials and methods**

76 *2.1. Samples*

77 A plate of 2 mm thickness of pure polytetrafluoroethylene PTFE (Approflon, France)
78 was used to cut out circular samples with a manual press equipped with a cookie cutter
79 of 10 mm in diameter. The samples were polished with an automatic polishing machine
80 until $0.055\ \mu\text{m}$ arithmetic roughness (S_a) was obtained. After the polishing step, the
81 samples were washed with ethanol in an ultrasonic bath for 15 min and then dried
82 for 1 h in an oven at a temperature of 95°C . Contact angle measurements are then
83 realized with a semi-automatic goniometer (Krüss DSA25) by posing a drop of $5\ \mu\text{l}$
84 on the sample surface. For each sample, contact angle measurements are done in five
85 different areas. The values of contact angle were between 107° and 112° (see figure 1),
86 which is in agreement with the literature [27].

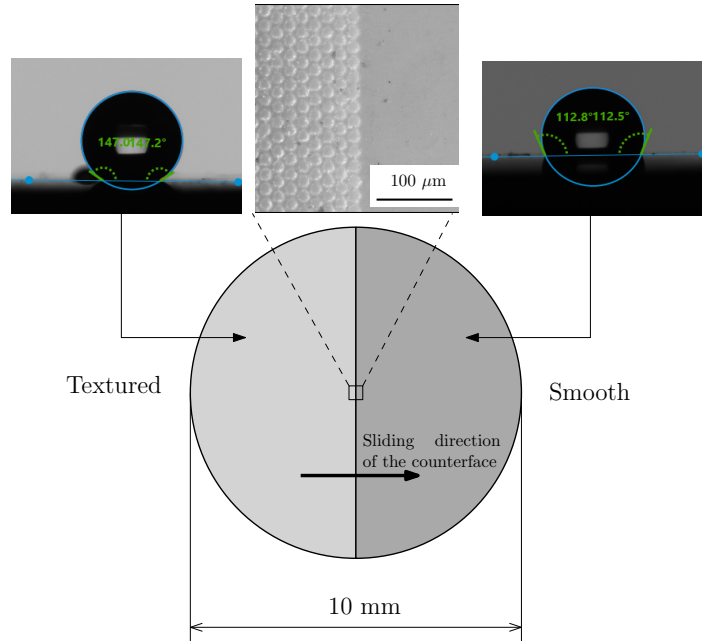


Figure 1. Example of half-textured sample with $20\ \mu\text{m}$ lateral texture size and sessile water drop images on the smooth and textured areas with respective contact angles (112.8° , 112.5°) and (147.0° , 147.2°).

87 2.2. Surface texturing

88 To increase the hydrophobicity and reach a superhydrophobic state, the surfaces of
 89 the PTFE samples were textured. To allow a better mobility of the water on the surface,
 90 the objective was to obtain a Cassie Baxter wetting state, when the water drop lies on
 91 the top of the asperities, and avoid the Wenzel wetting state, when the water drop fully
 92 wets the asperities. Restrictions need to be imposed on the geometry of the pattern to
 93 ensure that the Cassie Baxter will be the most favorable energetic state [28]. Moreover,
 94 the texture must withstand mechanical shear loading during the friction tests. Thus, it
 95 was decided to create a network of cavities rather than the slender pillars or ridges that
 96 are used in the literature [25]. In this case, the contact angle θ_{textured} for the Cassie Baxter
 97 state satisfies the relation:

$$\cos \theta_{\text{textured}} = f \cos \theta + f - 1, \quad (1)$$

98 where f is the ratio of the area of the top surface (out of the cavities) to the total area and
 99 θ the contact angle for the smooth surface. To maintain a minimum material thickness
 100 between the cavities, the surface fraction f cannot be lower than about 0.2. If $\theta \simeq 110^\circ$,
 101 then a contact angle of 150° is expected theoretically for a textured surface. The surface
 102 texture was manufactured with a femto-second laser (Manutech, France). The minimum
 103 texture lateral size that can be machined with the laser is $10\ \mu\text{m}$. A second set of samples
 104 with a lateral size of $20\ \mu\text{m}$ was also machined to obtain a better control of f and of
 105 the shape of the cavities. Figure 2 shows the topography measured with a white light
 106 interferometer (Taylor Hobson Talysurf CCI 6000) on a sample with a $10\ \mu\text{m}$ pattern size
 107 and on a sample with a $20\ \mu\text{m}$ pattern size. The average depth of the pattern is about $5\ \mu\text{m}$
 108 for the small texture and about $10\ \mu\text{m}$ for the large texture.

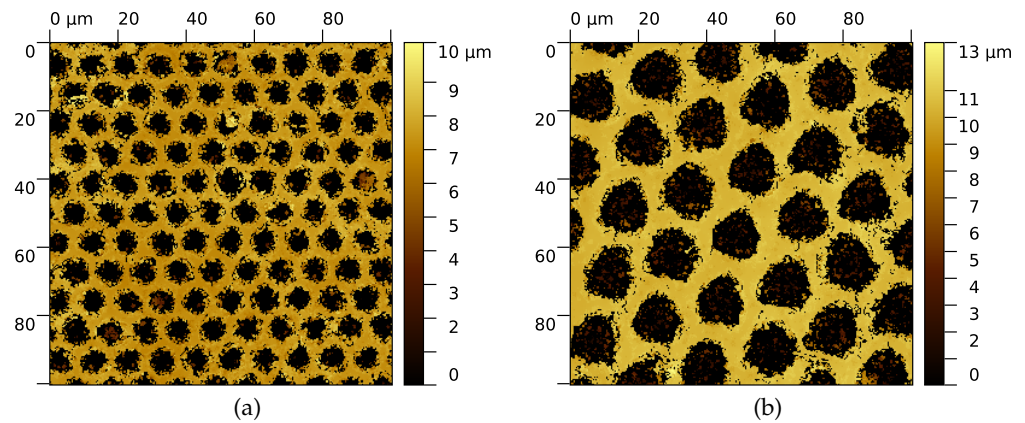


Figure 2. Surface topography of the samples measured by white light interferometry: (a) Sample with 10 μm lateral texture size. (b) Sample with 20 μm lateral texture size.

109 As proposed by Salant and Fortier [8], the samples were only partially textured to
 110 give a heterogeneous slip/no slip surface that will generate hydrodynamic lift between
 111 the sample and the counterface. Indeed, in hydrodynamic lubrication, the lubricant
 112 is drawn into the contact by the sliding movement of the surfaces. To maintain this
 113 lubrication regime, part of the surfaces must form a converging space so that the outlet
 114 section of the entrained fluid is smaller than the inlet. This design keeps the fluid
 115 film under pressure and creates a lift force that pushes the two surfaces apart. We
 116 were inspired by this principle by texturing only half of our samples. In this way, the
 117 lubricating film will pass through the textured part, in which the flow of the fluid will be
 118 facilitated by the slip, unlike the exit (the second half of the sample was kept smooth).
 119 This will create a lift force that will prevent contact of the two surfaces and will maintain
 120 a hydrodynamic lubrication regime throughout the friction test. The configuration of
 121 the half textured sample is presented in figure 1. Three samples of each texture were
 122 manufactured and tested.

123 2.3. Test rig and experimental conditions

124 The test rig that we used for these experiments is presented in figure 3 a) and
 125 schematised in figure 3 b). The tribometer is composed of an horizontal arm mounted
 126 on a frictionless air bearing allowing free vertical motion of the sample support. The
 127 polymer sample was glued to the arm of the tribometer. *Before the glue dries, the PTFE
 128 disk was put into the contact with the counter-face, that is a smooth glass disk, to ensure
 129 perfect alignment of the sample and the glass. After drying, a controlled load was
 130 applied by means of a calibrated mass. Some water was poured on the glass disk to
 131 lubricate the contact.* The textured part of the sample was placed upstream with respect
 132 to the direction of rotation of the disk, which allows the lubricant to pass through the
 133 textured part first. Once the contact is established, the glass disk is rotated by a motor
 134 mounted under the tribometer. A displacement sensor was mounted in front of a thin
 135 elastic beam that maintains the sample support. When the sliding starts, the elastic
 136 beam bends due to the friction resistance of the sample/disk contact. This bending
 137 displacement was measured by the displacement sensor and related to the frictional
 138 force of the contact by the stiffness of the setup measured prior to the experiments.

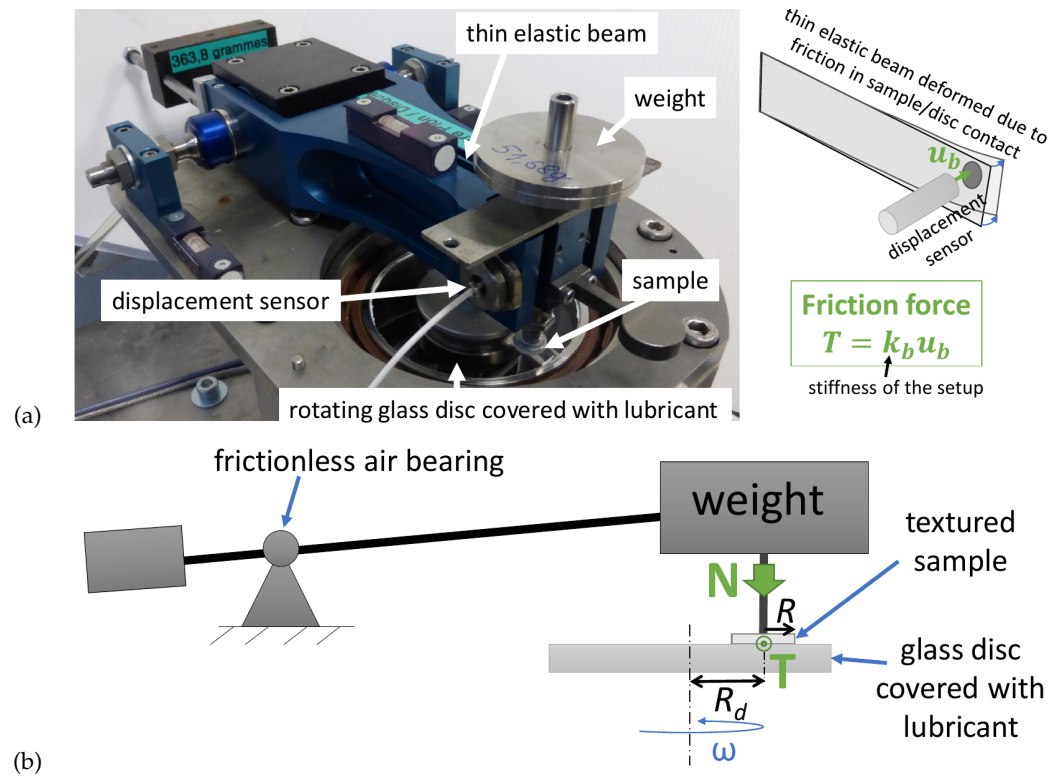


Figure 3. Presentation of the test rig : (a) Picture of the rig. (b) Principle of operation.

139 Several sliding conditions were tested by changing the sliding speed and normal
 140 load. The rotational speed ω of 100 rpm, 150 rpm and 200 rpm and the calibrated masses
 141 from 10g to 70g were used. The radial position of the sample on the disk was $R_d =$
 142 0.035 m. The test conditions are summarized in table 1. The averaged loading pressured
 143 calculated from the applied mass and the sample area is also indicated.

144 Each sample was used only once for each normal load and sliding speed combina-
 145 tion to avoid any wear of the surface texture. Sliding duration was set at 30 seconds. The
 146 friction coefficient presented later on was averaged on the last 25 seconds.

Table 1. Test conditions.

Parameter	Value
Sample material	PTFE
Rotating disk material	Glass
Lubricant	Water at 20°C
Rotational speed ω (rpm)	100, 150, 200
Applied mass (g)	10, 30, 50, 70
Corresponding averaged pressure (kPa)	1.3, 3.8, 6.4, 9.0

147 2.4. Simulation tool

148 A simulation tool was used to analyze the results of the test. The configuration
 149 of the studied problem is presented in figure 4. The sample of radius R is placed at
 150 distance h_0 from a flat surface moving along the x direction. A possibility of integrating
 151 a flatness defect of the sample was introduced into the model by introducing two radii
 152 of curvature R_1 and R_2 .

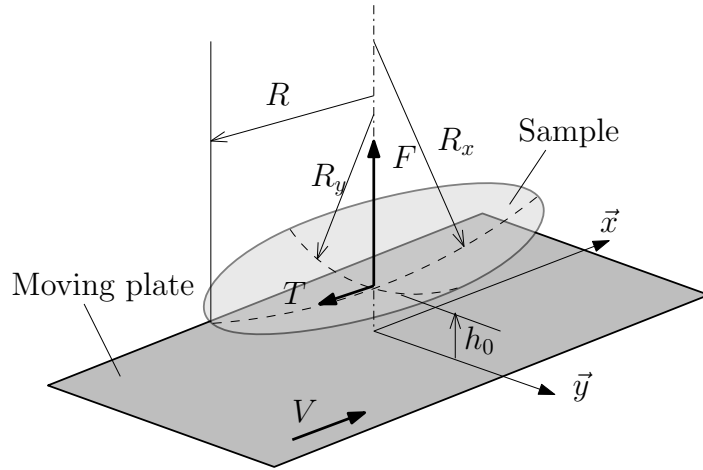


Figure 4. Configuration of the simulated problem.

It is assumed that the fluid flow between the sample and the moving surface is governed by the Reynolds equation. In addition, a mass conserving cavitation model is used [29], leading to:

$$F \frac{\partial}{\partial x} \left(\frac{h^3}{\mu} \frac{\partial D}{\partial x} \right) + F \frac{\partial}{\partial y} \left(\frac{h^3}{\mu} \frac{\partial D}{\partial y} \right) = 6V \left[\frac{\partial h}{\partial x} + (1 - F) \frac{\partial h D}{\partial x} \right] \quad (2)$$

where h is the local film thickness and μ the fluid viscosity. F is switch function and D a universal variable that is related to the pressure p of the fluid or its density ρ , depending if the fluid film is cavitated. In full film zones:

$$F = 1, \quad D = p, \quad \text{and} \quad \rho = \rho_0 \quad (3)$$

and in zones of cavitation:

$$F = 0, \quad D = \frac{\rho}{\rho_0} - 1, \quad \text{and} \quad p = p_{cav}. \quad (4)$$

153 In these equations, ρ_0 is the liquid density and p_{cav} is the cavitation pressure. The
 154 Reynolds equation was discretized by the finite difference method and the system of
 155 equations was solved by a direct LU decomposition method for sparse matrices. Once
 156 the pressure in the fluid domain was calculated, the normal force N and the friction
 157 force T on the sample were calculated.

158 3. Results

159 3.1. Sample characterization

160 The contact angle results for the textured surfaces are given in table 2. A representa-
 161 tive image of a water drop on a textured surface can be seen in figure 1. As expected, the
 162 texture significantly increased the contact angle that was initially close to 110° for the
 163 flat smooth PTFE surface. The contact angle of textured surfaces reached values close
 164 to, or higher than 150° . This value is considered to be the threshold, above which the
 165 behavior is superhydrophobic. Furthermore, the texture with a $20 \mu\text{m}$ lateral size gave
 166 better results because of better precision of the laser machining and better control of the
 167 surface fraction f .

Table 2. Contact angle of water drops on texture surfaces.

Sample	Spacing	Static angle
T10-1	10 μm	$133 \pm 1^\circ$
T10-2	10 μm	$143 \pm 2^\circ$
T10-3	10 μm	$145 \pm 2^\circ$
T20-1	20 μm	$147 \pm 2^\circ$
T20-2	20 μm	$142 \pm 2^\circ$
T20-3	20 μm	$153 \pm 3^\circ$

168 In addition to the contact angle characterization, the global shape of the samples
169 was measured with a 3D optical microscope (Alicona InfiniteFocus). It was then possible
170 to calculate the principal radii of curvature R_1 and R_2 of the surfaces of all of the samples
171 that we used. The results are presented in figure 5. These results show that the samples
172 were not perfectly flat, with a curvature radius of about 0.5 m. This curvature induced a
173 film thickness variation in the contact between the sample and the glass disk of several
174 tens of microns. It is noteworthy that this value is significantly larger than the texture
175 depth.

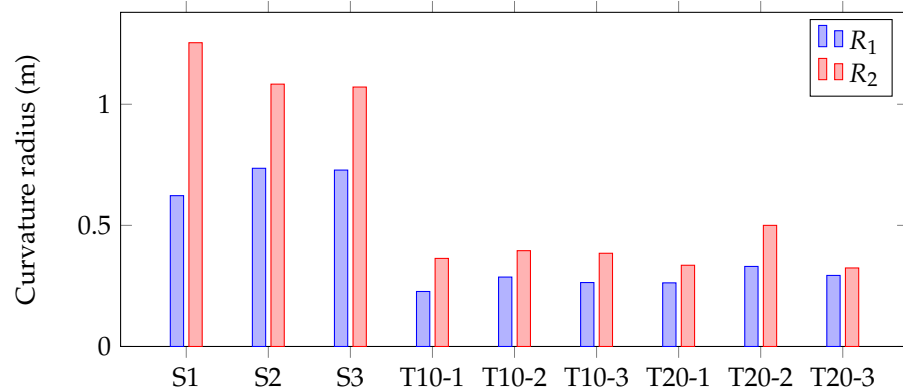


Figure 5. Principal curvature radii of the PTFE samples

176 3.2. Friction tests

177 Figure 6 a) presents typical tangential force signals as a function of the sliding
178 distance for one sample of each type (smooth, textured with a lateral spacing of 10
179 μm and textured with a lateral spacing of 20 μm). Even if the average value of the
180 tangential force is stabilized, all the three signals exhibits some oscillations at three
181 different frequency levels (see figure 6 b). The high frequency corresponds to noise on
182 the signal. The oscillation with a period of about 0.07 s is the flexural natural frequency
183 of the tribometer. The damping of the fluid film is not sufficient to vanish the vibration
184 during the test length (30s). Finally an oscillation with a longer period probably induced
185 by the revolution period of the disk (about 0.4 s) is also viewable. The signals are
186 averaged over 25 s to eliminate the effect of these time oscillations.

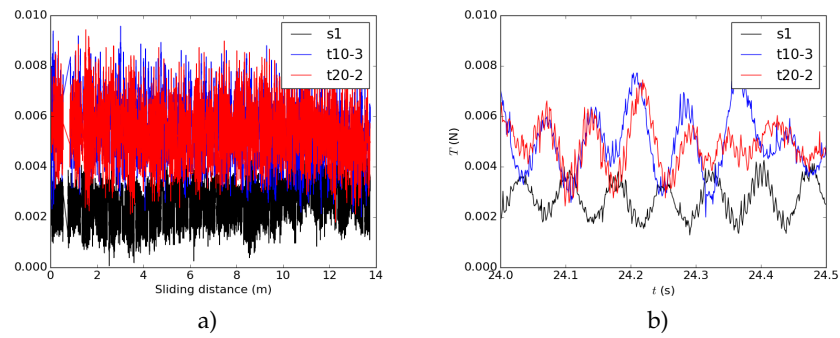


Figure 6. Measured tangential force as a function of the distance or time for three type of samples. The loading mass is 30 g and the rotational speed is 150 rpm. a) Tangential force versus sliding distance for full test recording b) Tangential force versus time during the last half second

The results of the tests presented in figure 7 are averaged over three samples of each category (smooth, textured with a lateral spacing of $10 \mu\text{m}$ and textured with a lateral spacing of $20 \mu\text{m}$). An error bar represents the variation among the three samples. The friction coefficient is the ratio of the friction force T over the normal load N . It is presented as a function of the duty parameter G , which is defined in the following way:

$$G = \frac{2\mu VR}{N} \quad (5)$$

187 where $V = R_d\omega$ is the linear sliding speed of the sample/disk contact.

188 To highlight the evolution of the friction, a power law was fitted to each set of results.
 189 For each sample family, the opacity of the markers is proportional to the applied load
 190 making it possible to identify the effect of speed and load independently. Increasing the
 191 load at a given speed makes the friction lower while increasing the speed leads at a given
 192 load to a higher friction. For each family of samples, the friction increased with G , which
 193 means that the lubrication regime is mainly hydrodynamic. The variations in friction
 194 coefficient obtained for each category can be related to the difference in shape within
 195 the samples (see figure 5). Unlike the expectations, the lowest friction was obtained
 196 with the smooth surfaces, while the $10 \mu\text{m}$ spacing textured surfaces gave the highest
 197 friction value. Although the surface texturing was expected to allow slip of the fluid
 198 on the surface by increasing the contact angle, the results revealed that this was not the
 199 case. One possible explanation of this surprising finding is that the flatness defects of the
 200 sample had an influence on the results. This hypothesis will be discussed and verified in
 201 the following section.

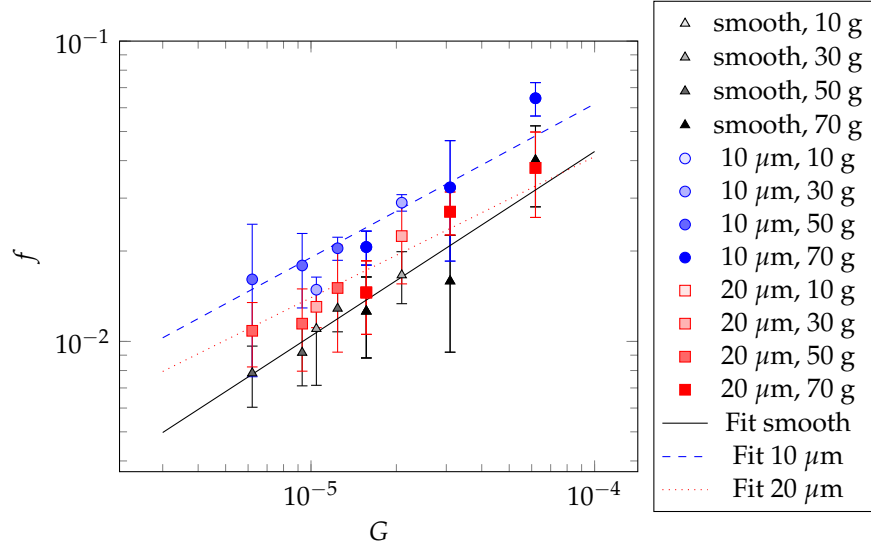


Figure 7. Measured friction coefficient as a function of the duty parameter G for three type of samples. The values are averaged from three samples of each set and the error bar is the standard deviation. The opacity of the symbols is proportional to the load level. A power law fit curve is presented for each category.

202 4. Discussion

203 4.1. Simulation of the effect of surface curvature

204 According to the lubrication theory, no hydrodynamic pressure can be generated
 205 between parallel flat surfaces. However, our results showed that a hydrodynamic lubri-
 206 cation regime can be reached with smooth samples. The hydrodynamic force is in fact
 207 generated by the surface residual curvatures due to the polishing process. In addition,
 208 this force depends on the surface curvature radii. This makes the comparison of the
 209 performance of different samples difficult because their surfaces are not identical. To
 210 highlight the effect of surface curvature, simulations were carried out on the configura-
 211 tion presented in figure 4. The simulations were performed for different values of
 212 the curvature radii R_x and R_y of the sample and for different values of the central film
 213 thickness h_0 . The parameters that were used in the simulations are given in table 3.

Table 3. Parameters used for the simulation of figure 8.

Parameter	Value
Viscosity μ (Pa.s)	0.001
Averaged sliding speed V (m.s ⁻¹)	1
Sample radius R (m)	0.005
Curvature radius R_x (m)	0.1 – 1
Curvature radius R_y (m)	0.1 – 1
Domain size (m)	0.012
Number of nodes	256 × 256
Cavitation pressure p_{cav} (Pa)	0

The calculated friction coefficient $f = \frac{T}{N}$ was presented as a function of the duty parameter G scaled by a shape factor:

$$G^* = G \times \left(\frac{\sqrt{R_x R_y}}{R} \right)^a \quad (6)$$

All of the simulation results with different surface curvatures were laid on the same line with the power law coefficient $a = 0.355$, as can be seen in figure 8. When presented as a function of this modified duty parameter G^* , the friction coefficient is independent on

the surface curvature. It is thus possible to fit the simulation results with a power law function:

$$f = 6.16 \times (G^*)^{0.62} \quad (7)$$

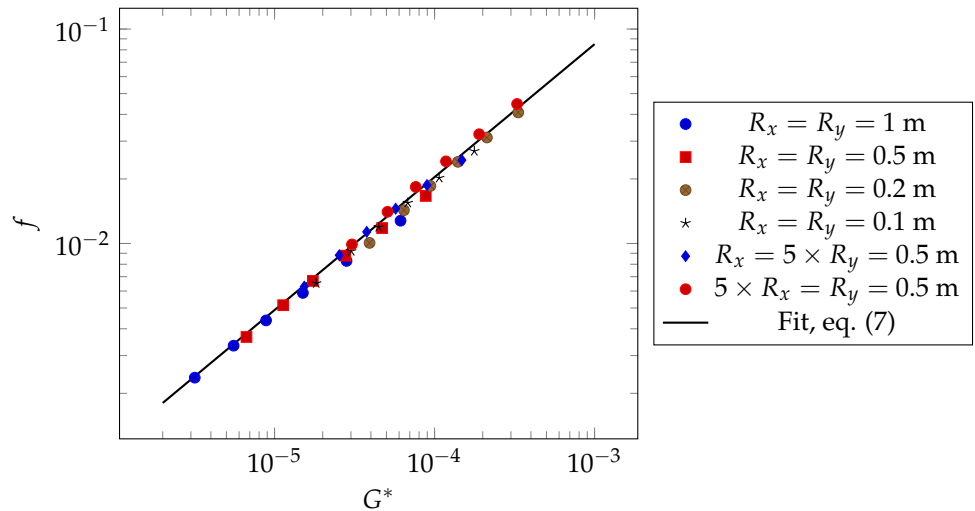


Figure 8. Simulated friction coefficient as a function of the modified duty parameter G^* for different values of the surface curvature radii. A power law curve has been fitted on the results.

214 4.2. Discussion of the experimental friction results

215 To remove the effect of the residual curvature of the samples, the friction coefficient
 216 is presented as a function of G^* in figure 9. The power law (7) obtained from simulations
 217 has also been added to the figure. It is interesting to see that the friction coefficient
 218 obtained with the smooth samples S2 and S3 is in good correlation with simulation law.
 219 Meanwhile, sample S1 gives a slightly lower friction. When the surfaces are textured, a
 220 significantly higher friction is obtained, except for a few conditions. This observation
 221 stands for the two configurations of texture. Although an increase of the hydrophobicity
 222 of the surfaces due to texturing was expected to provide a better sliding of the water and
 223 to reduce friction, the opposite is obtained here. This means that the slip of water does
 224 not take place.

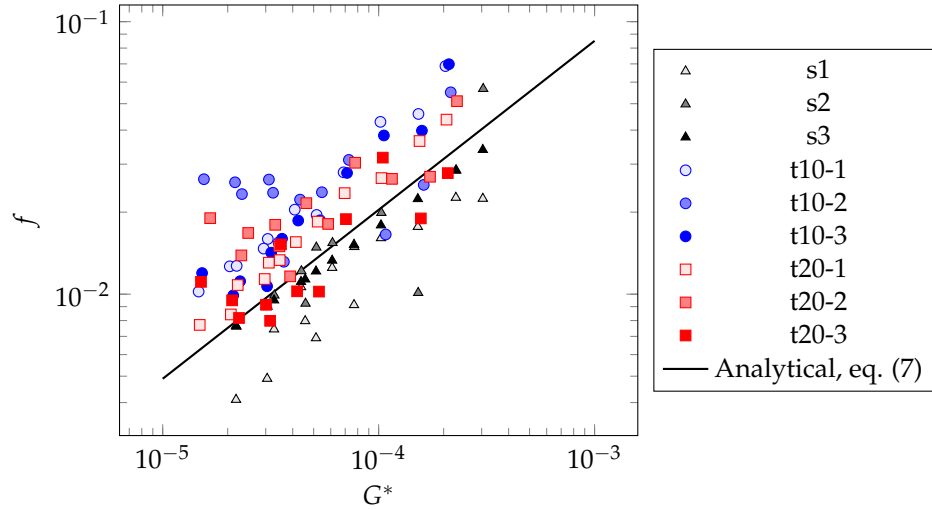


Figure 9. Friction coefficient as a function of the modified duty parameter G^* , Eq. (6) - Experimental results and comparison to the numerically fitted curve

225 An analysis of the results of the literature ([13,22,23,25]) where a friction decrease
 226 was obtained thanks to surface texture enhancing hydrophobicity shows that in all cases
 227 the texture was composed of pillars or ridges parallel to the flow direction. Even if an
 228 amount of air is maintained between the texture, the fluid flow was facilitated between
 229 the ridges and pillars. In our case, the texture is composed of cylindrical cavities. Even if
 230 these cavities are efficient in increasing hydrophobicity and can maintain the air trapped
 231 in the cavities, there is no easy path for the water flow.

In addition, during the simulations performed to obtain the results of figure 8, the maximum fluid pressure calculated in the fluid film varied between about 6.5 kPa and 270 kPa, depending on the value of G^* . This pressure would impact the interface between water and the air trapped in the cavities, as shown in figure 10. The curvature radius of the spherical interface is given by the Laplace equation:

$$R_c = \gamma \times \left(\frac{2}{p_\ell - p_g} \right) \quad (8)$$

where γ ($= 0.071 \text{ N.m}^{-1}$) is the water surface tension, p_ℓ is the liquid pressure and p_g is the gas pressure. The maximum pressure differential that can withstand the interface depends on the diameter of the hole and the value of the contact angle θ (see figure 10). It is thus possible to calculate a critical diameter d_c of a hole from the fluid pressure resulted from the simulations:

$$d_c = -\gamma \times \left(\frac{4 \cos \theta}{p_\ell - p_g} \right). \quad (9)$$

232 Using the pressure calculated in the simulations, it is found that d_c is in the range 0.36
 233 μm for the highest pressure value to 15 μm for the lowest pressure. The size of the
 234 texture used in the experiments is thus not small enough to ensure the stability of the
 235 water-air interface for all of the experimental conditions. It is thus possible for the water
 236 to fill the cavities, either partially or completely.

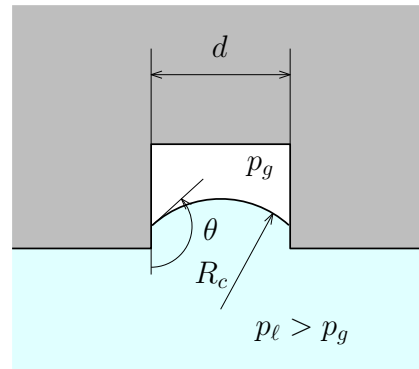


Figure 10. Effect of the liquid pressure on the air water interface shape.

237 Several papers [30,31] dedicated to the simulation of fluid flow over textured
238 surfaces with a shape ratio (texture depth to texture width) similar to our case have
239 demonstrated that flow vortices can be observed in the cavities, even at a very low
240 Reynolds number. More particularly, Mateescu et al. [30] showed that the viscous
241 dissipation in these vortices leads to an increase in drag or friction **even for Reynolds**
242 **number values tending to zero. The most important parameter for drag increase was**
243 **shown to be the ratio of cavities depth to film thickness.** Given that it is possible for
244 water to partially or completely fill the cavities due to the hydrodynamic pressure in
245 the liquid, the air-water interface can be destabilized thus creating water cavities (figure
246 11). The results of Mateescu et al. [30] suggest that some vortices can appear in our
247 samples and increase the friction. In this case, the texture would work as a labyrinth
248 seal, contrary to what was expected.

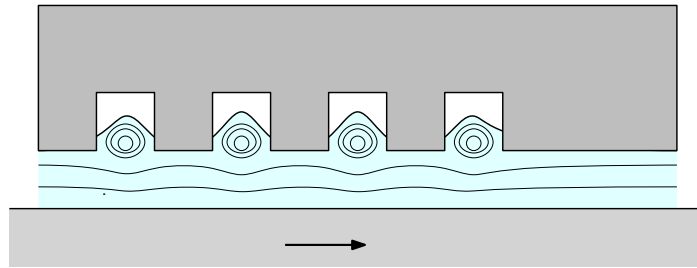


Figure 11. Vortices in the cavities increasing the sliding friction.

249 5. Conclusion

250 In this paper, the possibility to reduce friction in a hydrodynamic lubrication regime
 251 with superhydrophobic textured surfaces was experimentally investigated. PTFE disks
 252 were mechanically polished and textured with a femto second laser to create a hexagonal
 253 network of cylindrical cavities on a half of the sample's surface. The results showed that
 254 with cavities spacing of 10 and 20 μm , the hydrophobic character of the samples was
 255 increased with a contact angle up to 153°. Friction tests were conducted on these samples
 256 and compared to the results of smooth samples of the same material. In contrast to what
 257 was expected, these tests showed that the texture increased the friction coefficient. The
 258 numerical simulations with Reynolds flow showed that the observed effect could not
 259 be explained by the imperfect curvature of the sample surfaces. However, comparing
 260 our results with the literature provided a plausible explanation in that the fluid partially
 261 or completely filled the cavities due to high pressure in the contact. In addition, the
 262 literature supports the hypothesis that vortices could appear in the cavities, leading to
 263 an increase in friction due to the viscous dissipation. Indeed, the texture in our samples
 264 was applied by creating holes instead of the pillars used by other researchers. Our
 265 texture pattern was designed for better mechanical resistance of the surfaces to shear
 266 due to friction. However, it seems that this type of texture modifies the flow compared
 267 to the pillar texture, thus increasing the friction. This phenomenon can be avoided by
 268 using smaller cavities (sub-micron scale), which would imply the need to change the
 269 machining process.

270 **Author Contributions:** Conceptualization, O.S. and N.B.; methodology, H.J., O.S. and N.B.; soft-
 271 ware, H.J. and N.B.; validation, H.J., O.S. and N.B.; formal analysis, H.J., O.S. and N.B.; investigation,
 272 H.J.; writing and original draft preparation, H.J. and N.B.; writing, review and editing, H.J., O.S.
 273 and N.B.; visualization, H.J., O.S. and N.B.; supervision, O.S. and N.B.; project administration,
 274 N.B.; funding acquisition, N.B. All authors have read and agreed to the published version of the
 275 manuscript.

276 **Funding:** This work was supported by the French government program "Investissements d'Avenir"
 277 (LABEX INTERACTIFS, reference ANR-11-LABX-0017-01).

278 **Acknowledgments:** This work pertains to French government program "Investissements d'Avenir"
 279 (EUR INTREE, reference ANR-18-EURE-0010).

280 Abbreviations

281 The following abbreviations are used in this manuscript:

282
 283 PTFE PolyTetreFluoroEthylene

References

1. Holmberg, K.; Erdemir, A. Influence of tribology on global energy consumption, costs and emissions. *Friction* **2017**, *5*, 263–284.
2. Gropper, D.; Wang, L.; Harvey, T.J. Hydrodynamic lubrication of textured surfaces: A review of modeling techniques and key findings. *Tribology International* **2016**, *94*, 509 – 529. doi:10.1016/j.triboint.2015.10.009.
3. Rosenkranz, A.; Grützmacher, P.G.; Gachot, C.; Costa, H.L. Surface Texturing in Machine Elements - A Critical Discussion for Rolling and Sliding Contacts. *Advanced Engineering Materials* **2019**, *21*, 1900194. doi:10.1002/adem.201900194.

4. Etsion, I.; Halperin, G. A Laser Surface Textured Hydrostatic Mechanical Seal. *Tribology Transactions* **2002**, *45*, 430–434.
5. Dingui, K.; Brunetière, N.; Bouyer, J.; Adjemout, M. Surface Texturing to Reduce Temperature in Mechanical Seals. *Tribology Online* **2020**, *15*, 222–229. doi:10.2474/trol.15.222.
6. Spikes, H. The Half-wetted Bearing. Part 2: Potential Application in Low Load Contacts. *IMEchE, Part J, Journal of Engineering Tribology* **2003**, *217*, 15–26.
7. Spikes, H. The Half-wetted Bearing. Part 1: Extended Reynolds Equation. *IMEchE, Part J, Journal of Engineering Tribology* **2003**, *217*, 1–14.
8. Salant, R.; Fortier, A. Numerical Analysis of a Slider Bearing with a Heterogeneous Slip/No-Slip Surface. *Tribology Transactions* **2004**, *47*, 328–334, [<http://dx.doi.org/10.1080/05698190490455348>]. doi:10.1080/05698190490455348.
9. Wu, C.; Ma, G.; Zhou, P.; Wu, C. Low friction and high load support capacity of slider bearing with a mixed slip surface. *Journal of Tribology* **2006**, *128*, 904–907. doi:10.1115/1.2345419.
10. Fatu, A.; Maspeyrot, P.; Hajjam, M. Wall slip effects in (elasto) hydrodynamic journal bearings. *Tribology International* **2011**, *44*, 868–877. doi:doi.org/10.1016/j.triboint.2011.03.003.
11. Zhu, Y.; Granick, S. Limits of the Hydrodynamic No-Slip Boundary Condition. *Phys. Rev. Lett.* **2002**, *88*, 106102. doi:10.1103/PhysRevLett.88.106102.
12. Schnell, E. Slippage of water over nonwetable surfaces. *Journal of applied physics* **1956**, *27*, 1149–1152.
13. Kunert, C.; Harting, J. Roughness Induced Boundary Slip in Microchannel Flows. *Phys. Rev. Lett.* **2007**, *99*, 176001. doi:10.1103/PhysRevLett.99.176001.
14. Huang, D.M.; Sendner, C.; Horinek, D.; Netz, R.R.; Bocquet, L. Water Slippage versus Contact Angle: A Quasiuniversal Relationship. *Phys. Rev. Lett.* **2008**, *101*, 226101. doi:10.1103/PhysRevLett.101.226101.
15. Choo, J.; Spikes, H.; Ratoi, M.; Glovnea, R.; Forrest, A. Friction reduction in low-load hydrodynamic lubrication with a hydrophobic surface. *Tribology International* **2007**, *40*, 154–159. First International Conference on Advanced Tribology (iCAT 2004), doi:doi.org/10.1016/j.triboint.2005.09.006.
16. Guo, L.; Wong, P.; Guo, F. Correlation of contact angle hysteresis and hydrodynamic lubrication. *Tribology Letters* **2015**, *58*, 45.
17. Guo, L.; Wong, P.; Guo, F. Identifying the optimal interfacial parameter correlated with hydrodynamic lubrication. *Friction* **2016**, *4*, 347–358. doi:10.1007/s40544-016-0131-9.
18. Lin, W.; Klein, J. Control of surface forces through hydrated boundary layers. *Current Opinion in Colloid & Interface Science* **2019**, *44*, 94–106. Memorial Volume, doi:https://doi.org/10.1016/j.cocis.2019.10.001.
19. Rosenhek-Goldian, I.; Kampf, N.; Klein, J. Trapped Aqueous Films Lubricate Highly Hydrophobic Surfaces. *ACS Nano* **2018**, *12*, 10075–10083, [<https://doi.org/10.1021/acsnano.8b04735>]. PMID: 30252440, doi:10.1021/acsnano.8b04735.
20. Bhushan, B. Biomimetics: Lessons from Nature - An Overview. *Philosophical Transactions of the Royal Society A* **2009**, *367*, 1445–1486.
21. Law, K.Y.; Zhao, H. *Surface Wetting - Characterization, Contact Angle, and Fundamentals*; Springer, 2016.
22. Ou, J.; Perot, B.; Rothstein, J.P. Laminar drag reduction in microchannels using ultrahydrophobic surfaces. *Physics of Fluids* **2004**, *16*, 4635–4643, [<https://doi.org/10.1063/1.1812011>]. doi:10.1063/1.1812011.
23. Choi, C.H.; Kim, C.J. Large Slip of Aqueous Liquid Flow over a Nanoengineered Superhydrophobic Surface. *Phys. Rev. Lett.* **2006**, *96*, 066001. doi:10.1103/PhysRevLett.96.066001.
24. Srinivasan, S.; Choi, W.; Park, K.C.; Chhatre, S.S.; Cohen, R.E.; McKinley, G.H. Drag reduction for viscous laminar flow on spray-coated non-wetting surfaces. *Soft Matter* **2013**, *9*, 5691–5702.
25. Solomon, B.R.; Khalil, K.S.; Varanasi, K.K. Drag reduction using lubricant-impregnated surfaces in viscous laminar flow. *Langmuir* **2014**, *30*, 10970–10976.
26. Küper, S.; Stuke, M. Ablation of polytetrafluoroethylene (Teflon) with femtosecond UV excimer laser pulses. *Applied Physics Letters* **1989**, *54*, 4–6.
27. Dann, J. Forces involved in the adhesive process: I. Critical surface tensions of polymeric solids as determined with polar liquids. *Journal of Colloid and Interface Science* **1970**, *32*, 302–320.
28. Bittoun, E.; Marmur, A. Optimizing Super-Hydrophobic Surfaces: Criteria for Comparison of Surface Topographies. *Journal of Adhesion Science and Technology* **2009**, *23*, 401–411, [<https://doi.org/10.1163/156856108X369958>]. doi:10.1163/156856108X369958.
29. Payvar, P.; Salant, R. A Computational Method for Cavitation in a Wavy Mechanical Seal. *Journal of Tribology* **1992**, *114*, 199–204.
30. Mateescu, G.; Ribbens, C.J.; Watson, L.T.; Wang, C.Y. Effect of a sawtooth boundary on Couette flow. *Computers & Fluids* **1999**, *28*, 801–813. doi:https://doi.org/10.1016/S0045-7930(98)00034-6.
31. Arghir, M.; Roucou, N.; Helene, M.; Frene, J. Theoretical Analysis of the Incompressible Laminar Flow in a Macro-Roughness Cell. *Journal of Tribology* **2003**, *125*, 309–318, [https://asmedigitalcollection.asme.org/tribology/article-pdf/125/2/309/5672660/309_1.pdf]. doi:10.1115/1.1506328.